iScience

CellPress
OPEN ACCESS

Article

The virtual multiple sclerosis patient

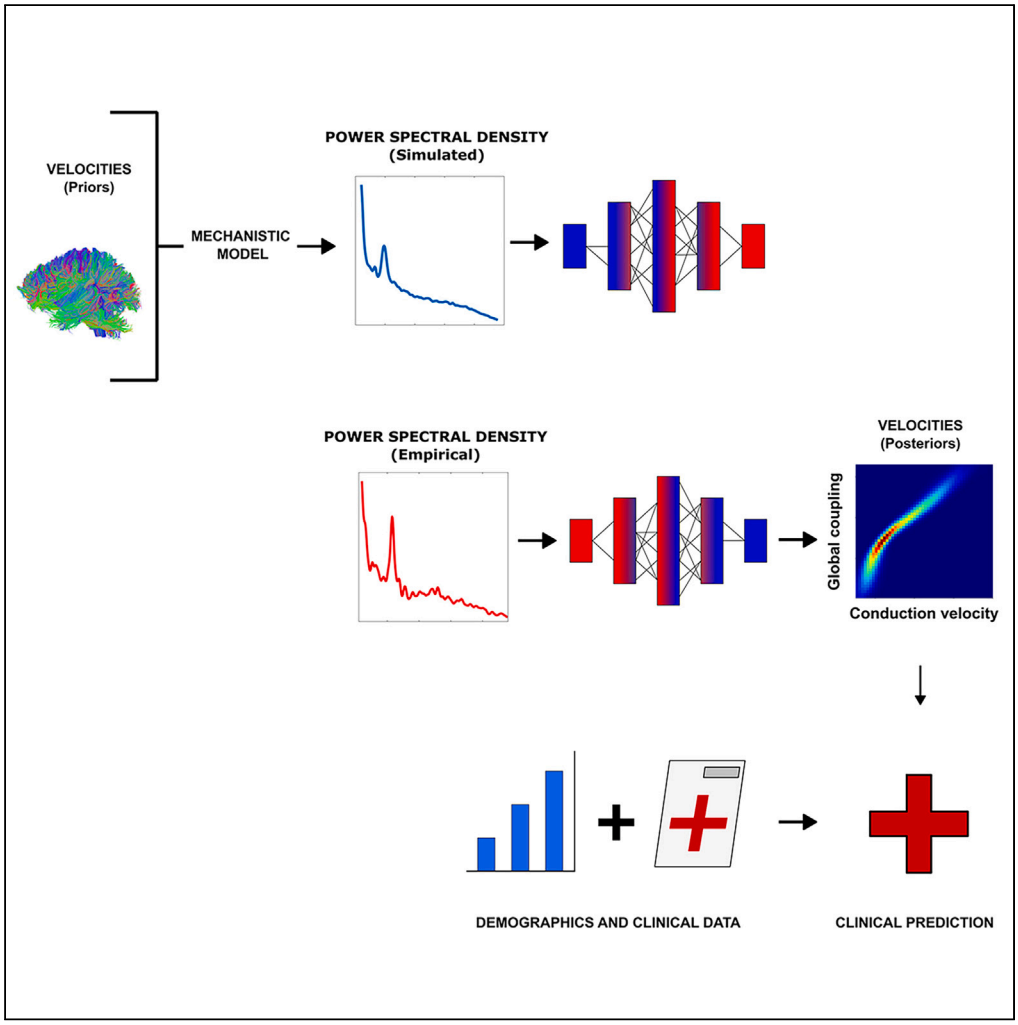

P. Sorrentino, A. Pathak, A. Ziaeemehr, ..., G. Sorrentino, V. Jirsa, M. Hashemi

pierpaolo.sorrentino@univ-amu.fr

Highlights

We integrate DTI and MEG data into personalized models of multiple sclerosis

Likelihood-free inference is used to estimate individualized conduction delays

Clinical prediction power: the inferred delays outperform structural damage

Sorrentino et al., iScience 27, 110101
July 19, 2024
https://doi.org/10.1016/j.isci.2024.110101

iScience

CellPress
OPEN ACCESS

Article

The virtual multiple sclerosis patient

P. Sorrentino,[1,2,9,*] A. Pathak,[3] A. Ziaeemehr,[1] E. Troisi Lopez,[4,5] L. Cipriano,[4,5] A. Romano,[4,5] M. Sparaco,[6] M. Quarantelli,[7] A. Banerjee,[3] G. Sorrentino,[4,5] V. Jirsa,[1,8] and M. Hashemi[1,8]

SUMMARY

Multiple sclerosis (MS) diagnosis typically involves assessing clinical symptoms, MRI findings, and ruling out alternative explanations. While myelin damage broadly affects conduction speeds, traditional tests focus on specific white-matter tracts, which may not reflect overall impairment accurately.

In this study, we integrate diffusion tensor immaging (DTI) and magnetoencephalography (MEG) data into individualized virtual brain models to estimate conduction velocities for MS patients and controls. Using Bayesian inference, we demonstrated a causal link between empirical spectral changes and inferred slower conduction velocities in patients. Remarkably, these velocities proved superior predictors of clinical disability compared to structural damage.

Our findings underscore a nuanced relationship between conduction delays and large-scale brain dynamics, suggesting that individualized velocity alterations at the whole-brain level contribute causatively to clinical outcomes in MS.

INTRODUCTION

Multiple sclerosis (MS) is an inflammatory disease of the human central nervous system.[1] While the etiology of the disease remains unknown to this day, structural magnetic resonance imaging has added to our understanding by allowing *in vivo*, non-invasive quantification of damage.[2] The underlying assumption was that patients with greater lesion load would be clinically worse than those with a smaller lesion load, and patients with more new lesions would be clinically more compromised than those without as many new lesions.[3] However, converging evidence showed otherwise, showing that lesion load alone remains a poor predictor of clinical outcome,[4–7] which makes it more difficult to utilize the lesion load in clinical practice and even as a biomarker in clinical trials. This explanatory gap points to the existence of more complex mechanisms, i.e., "hidden variables", that mediate the causal relationship between structural damage and clinical disability in MS. Multiple potential mechanisms (i.e., "candidate variables") and explanations have been attempted, but failed to provide a convincing, overarching understanding of the phenomenon.[3]

In the context of systems neuroscience, the brain is typically conceptualized as a complex dynamical network, whereby the accurate causal prediction on the effect(s) of a perturbation (e.g., a lesion) is challenging due to nonlinear interactions between functional units and consequently, the absence of one-to-one correspondence between structure and function.[8–10] Hence, we would not expect the lesion load to directly predict the final behavior outcome (i.e., the clinical condition). In particular, lesions in MS (especially in the early phases, and except for the primary progressive forms) are believed to relate to attacks from the immune system to the myelin sheath, which in turn manifest themselves as slower conduction velocities[11] (i.e., higher delays in the propagation of impulses traveling across the white-matter bundles). Prolonged visual evoked potential (VEP) latencies were in turn associated with poorer performance in multiple cognitive domains.[12] Recent evidence confirmed that there are widespread augmented delays across the brain in MS patients as compared to healthy controls.[13] Importantly, there is a wide body of statistical mechanics literature that is concerned with the behavior of complex networks as a function of the delays.[14,15] As such, one can estimate analytically and/or numerically how augmented delays would affect the overall network organization (specifically in terms of frequencies of network oscillations).[16–18] In particular, we focus on the fact that a shift in the power spectra has been observed in MS, whereby patients with MS show lower power in the alpha frequency band (8–13 Hz) and a shift in the peak frequency toward slower frequencies.[19–21] Even during tasks, alpha rhythms are most prominently affected in MS.[22]

In this paper, we hypothesize that the velocities (or, mathematically, the inverse of the delays) that are induced by the damage to the myelin in MS are responsible for the observed specific changes in power spectrum, which in turn would be better predictors of clinical disability

[1]Institut de Neurosciences des Systèmes, Aix-Marseille Université, Marseille, France
[2]Institute of Applied Sciences and Intelligent Systems, National Research Council, Pozzuoli, Italy
[3]National Brain Research Centre, Manesar, Gurgaon, Haryana, India
[4]Department of Motor Sciences and Wellness, Parthenope University of Naples, Naples, Italy
[5]Institute for Diagnosis and Cure Hermitage Capodimonte, Naples, Italy
[6]Department of Advanced Medical and Surgical Sciences, University of Campania Luigi Vanvitelli, Caserta, Italy
[7]Biostructure and Bioimaging Institute, National Research Council, Naples, Italy
[8]Senior author
[9]Lead contact
*Correspondence: pierpaolo.sorrentino@univ-amu.fr
https://doi.org/10.1016/j.isci.2024.110101

Table 1. Features of the multiple sclerosis cohort

	CONTROLS	MS	*p* value
Age (years)	45.8 (±11)	44.9 (±9.9)	0.8
Education (years)	13.6 (±3.8)	13.8 (±5)	0.9
Gender (m/f)	6/14	6/12	0.3
Disease duration (months)	–	187.7 (±131.8)	–
EDSS (mean +SD)	–	4.5 (±1.9)	–
SMDT (mean +SD)	–	40.3 (±13)	–
FSS (mean +SD)	–	36.1 (±14)	–
BDI (mean +SD)	–	12.8 (±1.3)	–
LESION LOAD (mean +SD)	–	12959 (±12253) mm3	–

EDSS, Expanded Disability Status Scale; SDMT, Symbol Digit Modalities; FSS, Fatigue Severity Scale; BDI, Beck Depression Inventory; LL, lesion load.

(as opposed to the total lesion load *per se*). To test this hypothesis, we utilized a previously published dataset,[13] made of 18 patients with MS and 20 controls. The main features of the MS cohort are summarized in Table 1. All subjects underwent both an MEG and MRI scan, which included the estimation of the tractography. This way, we have access to the individual connectomes and to the large-scale activity (i.e., the source-reconstructed MEG signals) for each subject. The current work entails the construction of personalized *in silico* models to estimate the average velocities determining the underlying dynamics. Firstly, we tested in this dataset for the presence of the previously described shift in the alpha-frequency peak and the reduction of the alpha-band in the power-spectra in MS patients. Once this was confirmed, we used large-scale brain modeling[17] to show that, given the individual structural connectomes, such changes on the overall power-spectra could be theoretically expected by higher conduction velocities.[23] The large-scale brain network modeling approach emphasizes the whole-network character of the changes in the organization of brain activities, which provides a link between the underlying physiological mechanisms and the clinical disability.[24] Then, once such theoretical prediction was confirmed, we moved on to test if the subject-specific reduction of conduction velocities could be inferred using probabilistic machine-learning techniques, starting from the empirical MEG data and the connectomes.[25]

However, the parameter estimation of large-scale brain network models is a challenging task due to the large dimensionality of data and the complex dynamics in each brain area, driven by noise and network input, and the strength of relationships between variables and/or parameters.[26] These factors challenge even state-of-the-art optimization methods and Markov chain Monte Carlo sampling algorithms. To address these challenges, advanced machine learning algorithms designed for high-dimensional probabilistic models are required to efficiently estimate the unknown model parameters and the statistical relationships between variables, ideally including the uncertainty.[27] In this study, we used Bayesian inference for model inversion, which is a principled method for updating beliefs with the information provided by the observed data (new evidence) to quantify uncertainty over hidden variables. For the present study, a key goal was to infer patient specific average conduction velocities as the parameter that modulates power spectra in the alpha frequency band. To this end, we used simulation-based-inference (SBI)[28] to estimate the conduction velocities (and a scaling parameter) over the patient's structural information, with the aid of only forward (random) simulations. To efficiently carry out SBI, we employed state-of-the-art deep neural networks for conditional probability density estimation (*25*), which provide the posterior distribution of the individual averaged velocities conditioned on the individual power-spectra in the alpha band. If our hypothesis is correct, then the model inversion should provide us with estimated slower velocities for MS patients as compared to healthy controls. Finally, as explained earlier, we set out to test our last hypothesis, namely that individual velocities would be a better predictor of clinical disability as compared to the lesion load alone. To this end, we built a multilinear statistical model to predict individual clinical disability.[29] Besides other demographic and clinical features, we also included the total lesion load and the global atrophy as predictors. We added atrophy since this is a better predictor of disability progression and conversion to secondary forms.[30] Then, we added the individual average velocities that were inferred by the Bayesian model inversion. An overall summary of the pipeline is provided in Figure 1. Given our hypothesis, we expect that including the individual velocities should significantly improve the prediction of the individual clinical disability beyond the predictive power of the individual structural changes.

RESULTS

Empirical spectral differences between patients and controls

The PSDs were estimated using the Welch method for each participant, in order to identify group differences in spectral features. In particular, the analysis focused on the alpha band (8–13 Hz). Power spectral density (PSD) estimates were calculated using median across ROIs to obtain a median spectrum for each participant (Figure 2A). We chose the median due to the left-skewed shape of the modeled PSD.[17] For the empirical data, since the PSD shape is bell-shaped around the peak, the mean and median become equal. In line with earlier studies, we found robust differences in alpha features between MS patients and age-matched controls. A modest slowing of the peak alpha frequency was also observed upon visual inspection; however, this did not survive formal statistical testing (Figure 2B). Most strikingly, MS patients displayed significantly attenuated peak alpha amplitudes as compared to controls ($p < 0.01$) (Figure 2C). Furthermore, the total power in the alpha band, measured as the area under the PSD curve between 8 and 13 Hz, was significantly lower in MS patients ($p = 0.02$ Figure 2D). Visual inspection

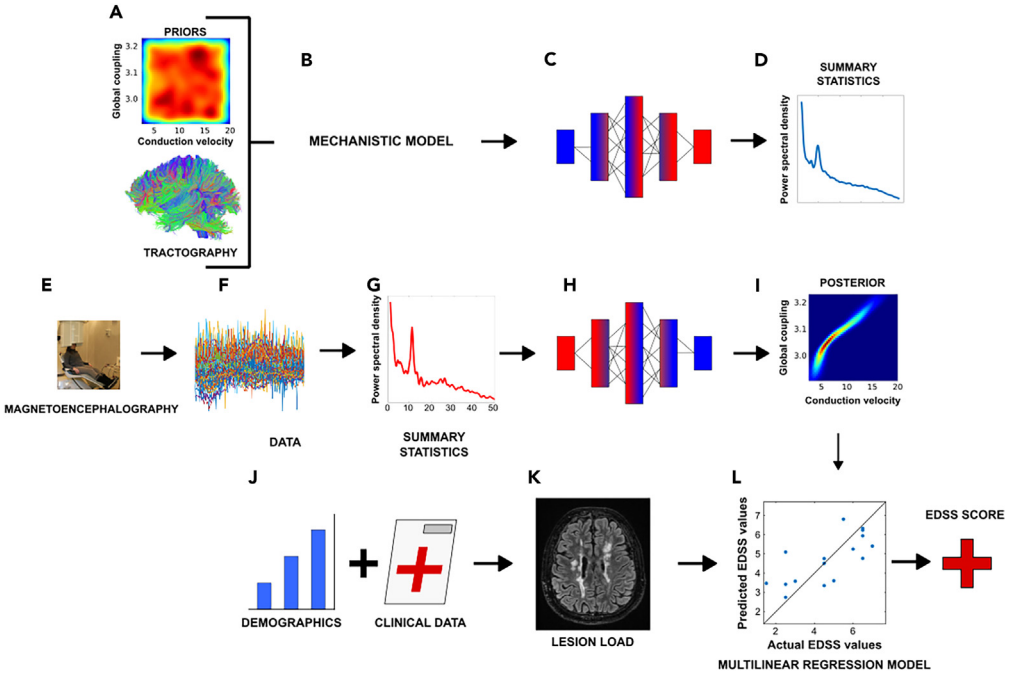

Figure 1. Overall pipeline

The patient undergoes non-invasive brain imaging (MRI, DTI). Based on these images, the subject-specific connectome is constructed. (A) The subject-specific tractography is then used to generate synthetic data by placing a mathematical model of neural activity at each region, (B) and incorporating global couplings and conduction velocities randomly drawn from physiologically plausible ranges as the prior. Subsequently, summary statistics of spectral power are extracted from the synthetic data. Probabilistic machine learning techniques are then employed to learn an invertible function (C) capable of relating parameters to spectral features, (D) along with their associated uncertainty. By providing the source-reconstructed magnetoencephalography data acquired from both MS patients and control subjects, (E and F) the spectral properties, serving as the data feature for model inversion, are calculated. (G) Then, posterior distributions for parameters (global coupling and conduction velocities) are approximated. (H) This leads to an efficient estimation of the most likely velocities given the observed summary statistics, namely spectral features. (I) Finally, based on the estimated velocities, demographic features, clinical data, (J) the total volume of lesions and global atrophy, (K) we built a multilinear model to predict individual clinical disability, (L) as quantified by the Expanded Disability Status Scale (EDSS).

also indicated modest differences in the theta and beta amplitude (not shown), however, these were not investigated further given the scope of this manuscript.

Numerical solution of the Stuart-Landau model

The complex interplay of coupling (indexed by G) and average conduction velocity (V) modulates the average peak frequency, peak power, and spectral distribution of oscillators in the network (see Figure 3). As shown previously, when operating in the partially synchronized regime, oscillators organize as metastable clusters, each oscillating at an emergent frequency and amplitude.[17,18,31] A similar frequency slowing has been previously explored for networks of phase oscillators like the Kuramoto model.[18,23] However, the Stuart-Landau model additionally allows for amplitude coupling.[17] In short, for weak couplings and large delays, the network resists synchronization and oscillators drift close to their natural frequencies (40 Hz). This state is characterized by relatively high gamma amplitudes, since all the power of the system is confined in the gamma band that is the natural frequency of the oscillators. In contrast, the network synchronizes at frequencies lower than the natural frequency ($\omega < \omega_0$) for stronger couplings, due to conduction delays.[18] Generally, for a given average conduction speed, stronger coupling is associated with the emergence of slower and lower amplitude oscillations. As one can observe in Figure 3, panels A and B, traversing leftwards along the heatmaps (that is, assuming progressively slower velocities or, equivalently, increasing delays) yields diminished peak frequency and power, provided the delays remain below the synchronization threshold. Robust low-frequency oscillations were observed in the $G = 800 - 1800$ and $V = 1 - 20\,\frac{m}{s}$ range. The peak amplitude, peak frequency and total alpha power (area under the PSD plot between 8 and 13 Hz were estimated for each simulation run and then averaged.

Model inversion and averaged velocities inference

Forward models predict the effects knowing the causes, whereas inverse models reveal the causes given the effects.[32] In this work, model inversion is used to estimate the most likely conduction velocities (and global coupling, i.e., the causes) in any individual given their spectral features (i.e., the effects). To obtain such estimation, we used a personalized generative brain model, where one can simulate the effect of changing conduction velocities on the spectral features of individual source-reconstructed MEG signals (via well-studied changes in network

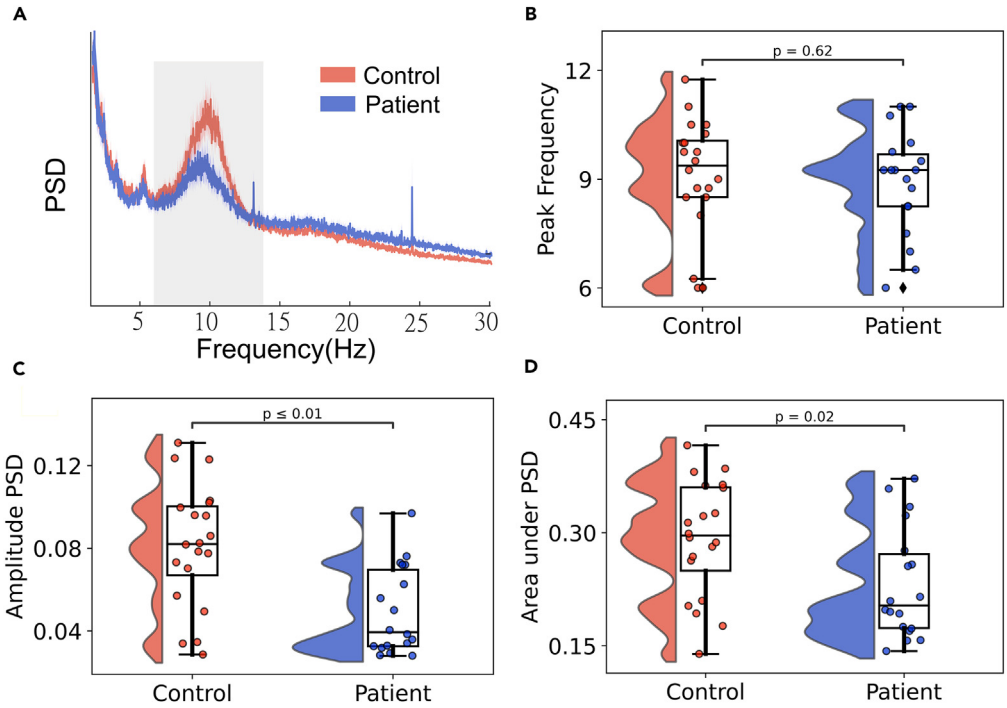

Figure 2. Empirical data features

Data features extracted from empirical MEG data for control and MS groups.

(A) Median power spectral density plotted for controls (red) and MS patients (blue) in the 1–30 Hz range. Shaded region represents the alpha band (8–13 Hz).

(B) The peak frequency shows non-significant changes in the control group relative to the patient group ($p = 0.62$).

(C) The amplitude of peak frequency illustrates a significant decrease from the control to the patient group ($p < 0.01$).

(D) The area under the PSD shows a significant decrease from the control to the patient group ($p = 0.02$).

synchronization).[18] Simulating the effects of different conduction velocities allows the estimation of their posterior distributions (i.e., what is the probability of a particular conduction velocity given the observed spectral features?). In this study, we utilized simulation-based inference (SBI) to perform Bayesian model inversion, which provides us with an efficient estimation of the posterior distributions of the conduction velocities (and global coupling). This results from updating the prior probability of having a plausible range of conduction velocities with the observed data (i.e., the spectral features), through the likelihood function, which in our case relies on personalized, large-scale brain models, and well-defined physical properties of networks of weakly coupled oscillators. In particular, we used ANNs for probability density estimation (i.e., Masked Autoregressive Flow) trained with a budget of 5000 model simulations.

Figure 4 shows the estimated posterior distributions over the whole-brain model parameters (the global coupling strength G, and the velocity V), by using SBI against the empirical PSD, pooled over the control and the patient groups. The posterior distribution of the parameter G, which scales the structural connectivity of subjects, demonstrated non-significant changes ($p = 0.87$), whereas the posterior distribution of averaged velocities V significantly decreased ($p < 0.01$) in MS patients as compared to the control group. Using synthetic data for model inversion allowed us to validate our inference process by knowing the ground-truth of the parameters being estimated (as demonstrated in Figure 5). Firstly, it can be seen that the predicted PSDs closely resemble the observed ones (Figure 5, panel A, blue and red, respectively). An example of observed and predicted MEG time-series averaged across brain regions are shown in Figure 5 panel B (by transforming the observation from the frequency-domain to the time-domain). Our result indicates that SBI accurately estimates a posterior distribution that narrows around the true parameters that generated the observed data (see Figure 5, panels C and D). This confirms that SBI can accurately capture relevant PSD features of MEG data, including the peak, amplitude and total power of the PSDs.

We also checked the accuracy of the estimated posterior distributions, in that increasing the number of simulations from 100 to 20000 led to progressively informative posteriors (i.e., less uncertainty in the estimation, as shown in Figure 5, panels C and D), with the maximum a posteriori closer to the ground-truth (i.e., the parameters used to generate the data). The joint posterior distribution (i.e., on the same probability space) between parameters G and V indicates a high correlation of 0.75 (Figure 5, panel E). In terms of computational cost, each model simulation took around 12 s (using just-in-time compilation in Python), which can be easily run on multiple central processing units (CPU)/graphics processing units (GPU) cores. Using a MAF model, the training took around 3 min, whereas generating 10000 samples from the posterior took only 1 s. We then performed sensitivity analysis using the estimated posterior from observation, which indicated that the model is more sensitive to the parameter V than G, as conveyed by the larger eigenvalue (by around 7 orders of magnitude), which reflects a larger gradient of the posterior for the averaged velocity (see Figure 5, panel F).

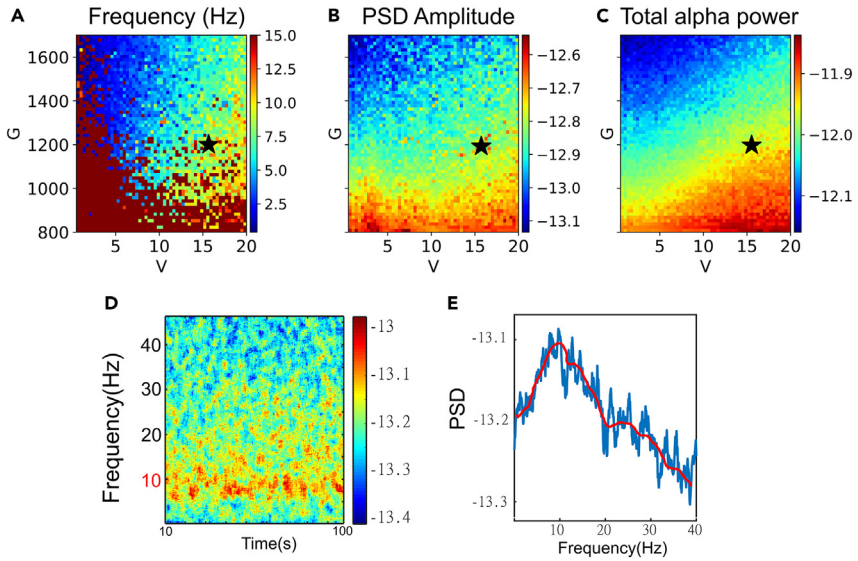

Figure 3. Model output

(A–C) Heatmaps indicate the median frequency, the median peak alpha PSD and the total alpha power, respectively, for the range $G \in [800, 1800]$ and $V \in [1,20]$. (D) Simulation output represented as the median spectrogram for $G = 1200$, $V = 16$ m/s (indicated as * in heatmaps) and (E) The corresponding median PSD (blue), for a given simulation run showing a peak in the alpha band (smoothed average in red). All PSDs reported in log-scale.

These results are consistent by normalizing the parameters G and V between zero and one (see Figure S1, in supplementary materials). In sum, our findings indicate that SBI on PSD at whole-brain level is efficient and accurate for Bayesian model inversion of MEG data.

Prediction of clinical outcome

We then moved on to test the validity of the inferred individual velocities in terms of prediction of the clinical disability. Please note that the Expanded Disability Status Scale (EDSS) score was not available for one patient and, hence, the prediction of the clinical outcome was carried out on 17 patients only. To this end, we built a multilinear model to predict clinical disability as measured by the EDSS scale. Gender, age, disease duration and lesion load (i.e., the total volume of lesions), and the inferred conduction velocities were considered as predictors. We found that the model performs well at predicting individual disability (R2 = 0.595, adjusted R2 = 0.41, see Figure 6, panel A). Adding the inferred velocities to the model significantly improves the predictive power over the EDSS ($p = 0.028$). The predicted vs. empirical EDSS values are shown in Figure 6, panel B. To test for the generalizability of our model, we used a leave-one-out cross-validation (LOOCV) scheme, whereby the model is trained, at each iteration, by excluding one patient, and then the EDSS is predicted for the patient that was not included in the training data. The results of the cross-validation are shown in the lower row of Figure 6 (i.e., the average results across all iterations are reported). In this case, the average R2 is 0.64, and adjusted R2 = 0.37, confirming the predictive power of the model. Again, adding the estimated speed to the model significantly improved the predictive power ($p = 0.04$). Note that the R2 reported for the cross-validation refers as the average value over all the instances of the cross-validations. Figure 6, panels C and F show the distribution of the residuals, confirming the appropriateness of using a linear model in this context. Finally, the values of variance inflation factor (VIF) were always below two for all

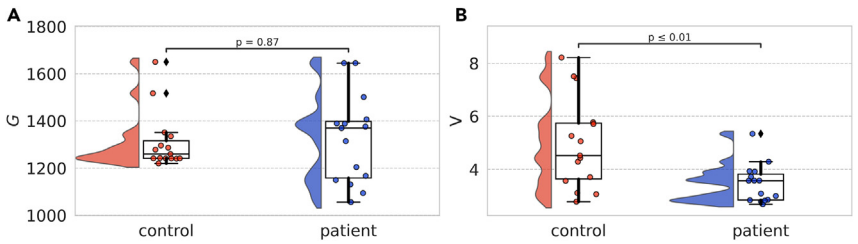

Figure 4. Estimated parameters for individuals

Estimated posterior distribution for two brain parameters from the PSD of the empirical MEG data, pooled over control and MS patient groups.

(A) The global coupling strength G shows non-significant changes ($p = 0.87$).

(B) The velocity parameter V significantly decreases in the control group relative to the patient group ($p < 0.01$).

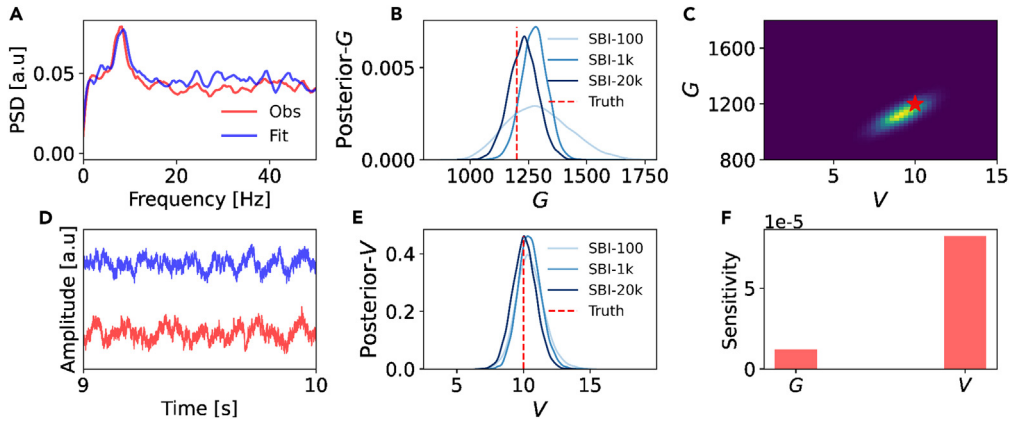

Figure 5. Diagnostics of the inference process for aggregated across individuals

(A and B) Observed (red) and predicted (blue) PSD of MEG data and corresponding time-series median average over brain regions, respectively.

(C and D) Inferred posterior distributions for the global coupling strength *G*, and the velocity *V*, respectively, given PSD features (amplitude, median frequency and total power). Increasing the number of simulations for training steps yields progressively tighter posteriors and, thus, a more accurate estimate.

(E) Joint posterior distribution between parameters *G* and *V* estimated from 20000 simulations (correlation = 0.75). The ground truth parameters are shown in red, the high-probability parameters in yellow, and the low-probability ones in blue.

(F) Sensitivity analysis using the estimated posterior, indicating stronger model sensitivity to *V* than to *G* (the Eigenvalues for *G* and *V* are 1.2e-05 and 8.2e-05, respectively).

predictors, showing that multicollinearity is unlikely to affect the model (not shown). When using brain atrophy instead of the lesion load as a predictor, we have found that the results remained consistent. Specifically, after cross-validation, the model displayed R2 = 0.56, and the estimated speeds as the only significant predictor (p = 0.046), see Figure S2.

DISCUSSION

In this manuscript we set out to test two related hypotheses. First, we hypothesized that slower conduction velocities across the brain manifest themselves as a reduction of the alpha power and a shift in the alpha peak at the level of the whole-brain frequency spectrum. Second, we hypothesized that the reduced velocities are predictive of the clinical disability in MS, above and beyond the clinical damage as measured by the lesion load. To test our hypotheses, we used source-reconstructed MEG data and tractographies from 18 MS patients and 20 healthy controls.[13] Most specifically, the area under the PSD in the alpha band, as well as the peak in the alpha band, are both lower in MS patients as compared to controls. This allowed us to hypothesize a direct link between the large-scale frequency spectrum and some well-known properties of weakly coupled oscillators, whereby the overall frequency of oscillation of a network is expected to decrease (with respect to the natural frequency of the oscillators) with growing delays.[18,23] With this in mind, we used an efficient mean-field based model of neuronal ensembles, namely Stuart-Landau oscillators,[33] coupled according to the subject-specific connectomes. We could then successfully reproduce *in silico*, for each individual, the expected shift in the peak spectral amplitude and the total power as a function of decreasing velocities. This provides a mechanistic account of the supposed link between the modifications in the individual large-scale frequency spectrum (i.e., our observed quantity) and the conduction delays (which cannot be observed directly in MS at the whole-brain level). The presence of such a mechanistic link allowed us to use this model to infer the individual average velocities, in the sense of performing Bayesian simulation-based inference in order to estimate the most likely individual delays, given the observed subject-specific large-scale frequency changes. Crucially, our large-scale model does not include any informative priors about the velocities (we used a uniform distribution in a biophysically plausible range). Despite this, the results of the model inversion clearly point to the fact that slower velocities (i.e., longer delays) become more likely given the observed changes in the power spectra in MS patients. In fact, the estimated velocities in MS patients are significantly slower than the ones estimated in the controls.

Subsequently, we used the inferred individual velocities to predict individual clinical impairment. In accordance with our hypothesis, the predictive power of our model significantly increases when we include the inferred velocities in the model. The lesion load was also included as a covariate. However, lesion load alone failed to predict most of the variance in clinical disability, in accordance with previous evidence.[3–5] We propose that averaged conduction velocities would be a relevant feature to explain clinical disability in MS. In that sense, we would interpret the poor performance of structural lesions at predicting clinical disability as the consequence of the fact that it is the velocities and not the structural lesion per se to be causing clinical disability. However, functional velocities (or the inverse of delays) depend on a multitude of different elements, including the size and the myelination of individual structural tracts, as well as the network in which each tract is embedded.[13] As such, it is evident that structural lesions would be a proxy of the functional damage that can only partly convey the "true" functional damage. In accordance with this view, the inferred averaged conduction velocities drastically outperform the lesion load at predicting clinical impairment. Furthermore, degenerative mechanisms are believed to be at play in MS alongside demyelinating

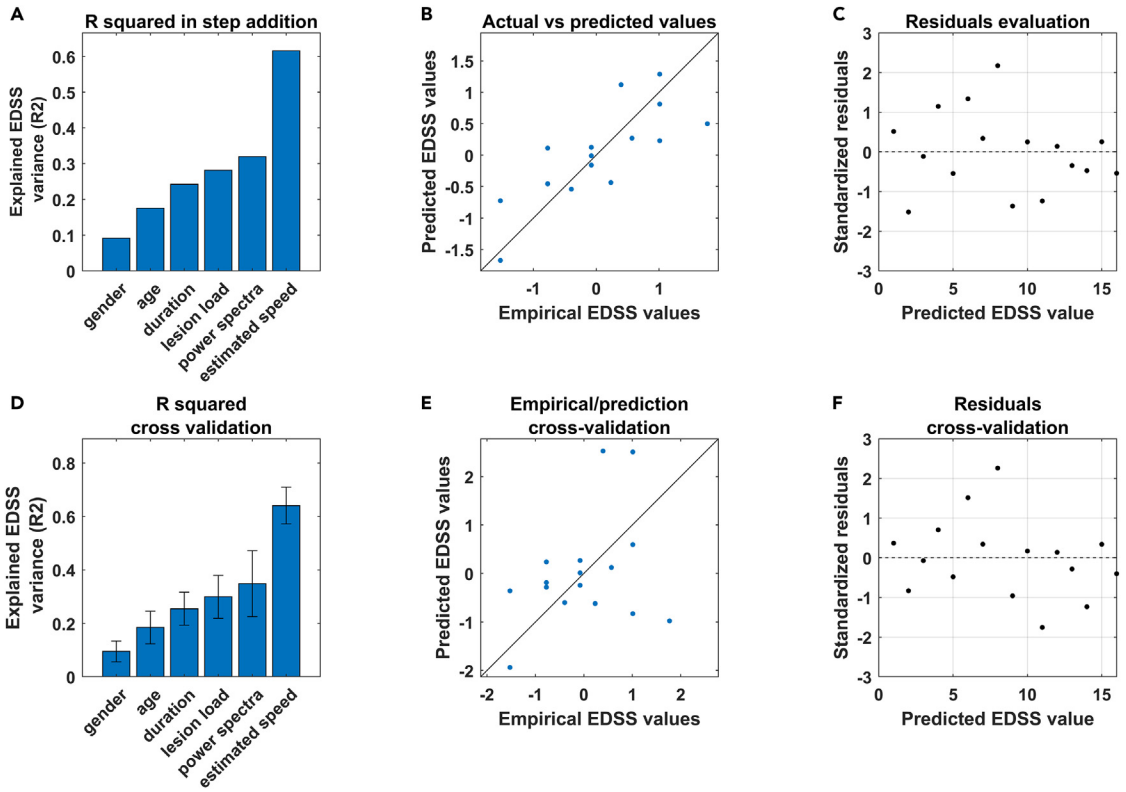

Figure 6. Prediction of clinical outcome

Multilinear regression model with leave-one-out cross-validation (LOOCV) performed to test the capacity of the estimated speed to predict the EDSS scores in MS patients.

(A and D) Variance explained by the additive model including five variables (i.e., gender, age, disease duration, lesion load, and estimated speed). Adding the estimated conduction velocities significantly increased the predictive power in both classical multilinear (panel A, $p = 0.028$) and cross-validated (panel D, $p = 0.0417$) models. Data are represented as mean ± SD.

(B and E) Empirical and predicted EDSS scores.

(C and F) standardized residuals of the model.

phenomena. This has been taken into account building a model using brain atrophy (a marker of degeneration). Even when taking this into account, the inferred global velocities add to the clinical prediction. In this sense, our results suggest a principled, physics-informed way to directly predict individual disability from the inferred velocities, thereby obtaining the most clinically relevant large-scale feature in MS by directly inferring the individual functional effects of the lesions instead. Finally, we have cross-checked the biological validity of the parameter V by exploring the predictive power of G, the global coupling (see Figure S3). In line with our hypothesis, G does not contribute predictive power to the multilinear model.

Furthermore, given that the lesion pattern is patient-specific in MS, the way edges are affected is most likely non-homogeneous even within each individual patient. However, in order to make the Bayesian inference computationally feasible, we adopted the simplifying assumption of homogeneous slowing of velocities across the brain of each-patient. This assumption might be reasonable given the recent evidence showing that the slowing of velocities across the brain of MS patients is not limited to the lesioned edges but, rather, it is widespread across the brain.[13] However, further improvement might be obtained including information about the individual lesions as model priors, as to introduce yet one more level of personalization in the large-scale models. This is feasible due to the flexibility of the Bayesian approach used in this study as compared to the classical optimization methods, which allows us to integrate the prior information in the inference process. For instance, it has been shown that measuring the prediction accuracy of a whole-brain network model with a higher level of information encoded in priors provides decisive evidence in favor of the true hypothesis regarding the degree of epileptogenicity across different brain regions.[34,35] To estimate the model parameters, optimization methods (within the frequentist approach) have been used in previous studies[17,36] by defining an objective (or a cost) function to score the performance of the model against the observed data. However, such a parametric approach results in only point estimation, and the optimization algorithms may easily get stuck in a local minimum, requiring multi-start strategies to address the potential multi-modalities. Moreover, the estimation depends critically on the form of the objective function defined for optimization. These issues can be solved by using Bayesian SBI. On the one hand, the traditional approaches for SBI[37] suffer from the curse of dimensionality and are sensitive to the ad-hoc choices (i.e., rejection thresholds, distance functions, and summary statistics), which

significantly affects both the computational efficiency and the accuracy; on the other hand, the SBI with the deep neural density estimator used in this study transforms a simple distribution conditioned on the data feature to obtain the full probability distribution of the target parameter, while dealing with non-linear and high-dimensional latent spaces and highly structured data (without the sensitivity to the tolerance level in the accepted/rejected parameter setting).

For this study, we have taken a minimalistic approach, in which we reduce the causal pathophysiological features t to be able to support the model inference to a maximum. Therefore, we collapsed the spatially distributed delay in one average delay and simplified the neural mass model. Stuart-Landau oscillators[33] were selected due to their sensitivity to variations in time delays. We acknowledge that our model does not explain all the features in empirical data, such as the characteristic 1/f phenomenon. Nevertheless, in striving to develop a model capable of capturing specific features of interest, we prioritize effectiveness (and, crucially, clinical relevance) over comprehensiveness. Attempting to reproduce every aspect of the data would lead to a high-dimensional model prone to degeneracy, obscuring the meaningful relationships between parameters and observed features and the causal driver. We feel like stressing that our model, while producing a clinical prediction, does not rule out other potential mechanisms that might be generating the same observed data. While changes in the conduction velocities appear the most reasonable explanation in MS, other potential mechanisms, such as changed in the excitation/inhibition ratio, in the 1/f properties, of microstructural alterations in the thalamic loops are all example at potential alternative mechanisms that might play a role. It will be important to check the feasibility of using electroencephalogram (EEG) instead of MEG, as this would contribute to the widespread applicability of our approach. The pipeline we propose (in terms of the building of a subject-specific, large-scale brain model, and the Bayesian model inversion to infer the individual averaged velocities) is available using the virtual brain (https://www.thevirtualbrain.org), a free, python-based tool designed for personalized large-scale models. However, the current work was carried out using a C++ implementation designed for high performance computing, to accelerate SBI by parallelizing processes.

In conclusion, we propose a principled way to link the most relevant physiopathological feature in MS, namely the slower conduction velocities across the brain network induced by myelin damage, to a large-scale observable quantity, that is the modification of the frequency spectrum. We then merged structural resonance, source-reconstructed MEG data, and a model of the large-scale brain using state-of-the-art deep learning algorithms, in order to infer the subject-specific median conduction velocities. Finally, we use the inferred conduction velocities in order to predict individual disability. Thus, our work paves the way to a principled application of personalized large-scale models in MS. Furthermore, from a more pathophysiological viewpoint, our results quantify the potential mechanisms (i.e., lower conduction velocities) through which structural damage would provoke large-scale changes in brain activity and, in turn, clinical impairment. The procedures described in this paper are the object of a deposited request for a patent.

Limitations of the study

Importantly, while promising, our results need to be replicated in larger multimodal, multicentric cohorts, to check that they are not specific to this particular dataset. However, we note that provided that the goodness of the personalization is quantified by the shrinkage of the posterior from prior, and by the study of the degeneracy, the small sample size does not affect the assessment of the personalization within each individual participant. Furthermore, a separate study should be used to compare the predictive power of the inferred velocities as compared to that of the "black holes" and, more in general, to other structural changes that might be related to different pathophysiological mechanisms (as opposed to neurodegeneration). Moreover, note that we have used ROI-to-ROI structural connectivity, which counts the structural connections between ROI pairs, including the indirect pathways. One should consider that some bias might be introduced using this technique, and robustness to different algorithms for tractography estimations will have to be explored. Also, using a 3T MRI scanner is needed to better inform the model with personalized data, since the resolution of the image might affect the personalization. Larger-samples will be needed to validate our approach across different populations and, generally, to deduce the validity of our approach within the general population. Finally, the reader should keep in mind that we aim at inferring an aggregate measure of the conduction velocities across the whole brain, which disregards the spatiotemporal structure of the data, and we focused solely on eyes-closed acquisitions. In fact, more information might be retrieved from these data (or a combination thereof).

STAR★METHODS

Detailed methods are provided in the online version of this paper and include the following:

- KEY RESOURCES TABLE
- RESOURCE AVAILABILITY
  - Lead contact
  - Materials availability
  - Data and code availability
- EXPERIMENTAL MODEL AND STUDY PARTICIPANT DETAILS
- METHOD DETAILS
  - MRI acquisition and processing
  - MEG pre-processing
  - Source reconstruction
  - Power-spectra estimation

SUPPLEMENTAL INFORMATION

Supplemental information can be found online at https://doi.org/10.1016/j.isci.2024.110101.

ACKNOWLEDGMENTS

The work was supported by the EBRAINS Italy nodo Italiano grant, CUP B51E22000150006, and by the European Union's Horizon 2020 research and innovation program under grant agreement No. 101147319 (EBRAINS 2.0 Project), No. 101137289 (Virtual Brain Twin Project), and ANR-22-PESN-0012 (France 2030 program). A.P. and A.B. were supported by NBRC core funds. A.B. was supported by Ministry of Youth Affairs and Sports, Government of India, Award ID: F.NO. K-15015/42/2018/SP-V, NBRC Flagship program, Department of Biotechnology, Government of India, Award ID: BT/MED-III/NBRC/Flagship/Flagship2019.

AUTHOR CONTRIBUTIONS

Conceptualization: S.P. and P.A.; methodology: S.P., P.A., and H.M.; investigation: S.P., P.A., Z.A., E.T.L., and R.A.; visualization: S.P. and Z.A.; supervision: S.P., B.A., G.S., J.V., and H.M.; data collection and curation: S.P., E.T.L., C.L., R.A., S.M., and Q.M.; data processing: S.P., P.A., Z.A., E.T.L., and H.M.; writing—original draft: S.P., P.A., Z.A., C.L., R.A., S.M., B.A., G.S., J.V., and H.M.; riting—review and editing: S.P., P.A., Z.A., E.T.L., C.L., R.A., S.M., B.A., G.S., J.V., and H.M.

DECLARATION OF INTERESTS

Pierpaolo Sorrentino, Viktor Jirsa, and Meysam Hashemi declare that a European patent has been deposited (N. 23315443.4).

Received: July 17, 2023
Revised: March 9, 2024
Accepted: May 22, 2024
Published: May 24, 2024

REFERENCES

1. Lassmann, H. (2018). Multiple Sclerosis Pathology. Cold Spring Harb. Perspect. Med. *8*, a028936. https://doi.org/10.1101/cshperspect.a028936.
2. Bakshi, R., Thompson, A.J., Rocca, M.A., Pelletier, D., Dousset, V., Barkhof, F., Inglese, M., Guttmann, C.R.G., Horsfield, M.A., and Filippi, M. (2008). MRI in multiple sclerosis: current status and future prospects. Lancet Neurol. *7*, 615–625. https://doi.org/10.1016/S1474-4422(08)70137-6.
3. Barkhof, F. (2002). The clinico-radiological paradox in multiple sclerosis revisited. Curr. Opin. Neurol. *15*, 239–245.
4. Nij Bijvank, J.A., Sánchez Aliaga, E., Balk, L.J., Coric, D., Davagnanam, I., Tan, H.S., Uitdehaag, B.M.J., van Rijn, L.J., and Petzold, A. (2021). A model for interrogating the clinico-radiological paradox in multiple sclerosis: Internuclear ophthalmoplegia. Eur. J. Neurol. *28*, 1617–1626. https://doi.org/10.1111/ene.14723.
5. Mollison, D., Sellar, R., Bastin, M., Mollison, D., Chandran, S., Wardlaw, J., and Connick, P. (2017). The clinico-radiological paradox of cognitive function and MRI burden of white matter lesions in people with multiple sclerosis: A systematic review and meta-analysis. PLoS One *12*, e0177727. https://doi.org/10.1371/journal.pone.0177727.
6. Truyen, L., van Waesberghe, J.H., van Walderveen, M.A., van Oosten, B.W., Polman, C.H., Hommes, O.R., Adèr, H.J., and Barkhof, F. (1996). Accumulation of hypointense lesions ("black holes") on T1 spin-echo MRI correlates with disease progression in multiple sclerosis. Neurology *47*, 1469–1476. https://doi.org/10.1212/WNL.47.6.1469.
7. Fouad, K., Popovich, P.G., Kopp, M.A., and Schwab, J.M. (2021). The neuroanatomical-functional paradox in spinal cord injury. Nat. Rev. Neurol. *17*, 53–62. https://doi.org/10.1038/s41582-020-00436-x.
8. Deco, G., Jirsa, V., McIntosh, A.R., Sporns, O., and Kötter, R. (2009). Key role of coupling, delay, and noise in resting brain fluctuations. Proc. Natl. Acad. Sci. USA *106*, 10302–10307. https://doi.org/10.1073/pnas.0901831106.
9. Sorrentino, P., Seguin, C., Rucco, R., Liparoti, M., Troisi Lopez, E., Bonavita, S., Quarantelli, M., Sorrentino, G., Jirsa, V., and Zalesky, A. (2021). The structural connectome constrains fast brain dynamics. Elife *10*, e67400. https://doi.org/10.7554/eLife.67400.
10. Madan Mohan, V., and Banerjee, A. (2022). A perturbative approach to study information communication in brain networks. Netw. Neurosci. *6*, 1275–1295. https://doi.org/10.1162/netn_a_00260.
11. Smith, K.J. (1994). Conduction properties of central demyelinated and remyelinated axons, and their relation to symptom production in demyelinating disorders. Eye (Lond) *8*, 224–237. https://doi.org/10.1038/eye.1994.51.
12. Covey, T.J., Golan, D., Doniger, G.M., Sergott, R., Zarif, M., Srinivasan, J., Bumstead, B., Wilken, J., Buhse, M., Mebrahtu, S., and Gudesblatt, M. (2021). Visual evoked potential latency predicts cognitive function in people with multiple sclerosis. J. Neurol. *268*, 4311–4320. https://doi.org/10.1007/s00415-021-10561-2.
13. Sorrentino, P., Petkoski, S., Sparaco, M., Troisi Lopez, E., Signoriello, E., Baselice, F., Bonavita, S., Pirozzi, M.A., Quarantelli, M., Sorrentino, G., and Jirsa, V. (2022). Whole-Brain Propagation Delays in Multiple Sclerosis, a Combined Tractography-Magnetoencephalography Study. J. Neurosci. *42*, 8807–8816. https://doi.org/10.1523/JNEUROSCI.0938-22.2022.
14. Jirsa, V.K., and Ding, M. (2004). Will a large complex system with time delays be stable? Phys. Rev. Lett. *93*, 070602. https://doi.org/10.1103/PhysRevLett.93.070602.
15. Banerjee, A., and Jirsa, V.K. (2007). How do neural connectivity and time delays influence bimanual coordination? Biol. Cybern. *96*, 265–278. https://doi.org/10.1007/s00422-006-0114-4.
16. Schnitzler, A., and Gross, J. (2005). Normal and pathological oscillatory communication in the brain. Nat. Rev. Neurosci. *6*, 285–296. https://doi.org/10.1038/nrn1650.
17. Cabral, J., Castaldo, F., Vohryzek, J., Litvak, V., Bick, C., Lambiotte, R., Friston, K., Kringelbach, M.L., and Deco, G. (2022). Metastable oscillatory modes emerge from synchronization in the brain spacetime

connectome. Commun. Phys. *5*, 184. https://doi.org/10.1038/s42005-022-00950-y.
18. Niebur, E., Schuster, H.G., and Kammen, D.M. (1991). Collective frequencies and metastability in networks of limit-cycle oscillators with time delay. Phys. Rev. Lett. *67*, 2753–2756. https://doi.org/10.1103/PhysRevLett.67.2753.
19. Cover, K.S., Vrenken, H., Geurts, J.J.G., van Oosten, B.W., Jelles, B., Polman, C.H., Stam, C.J., and van Dijk, B.W. (2006). Multiple sclerosis patients show a highly significant decrease in alpha band interhemispheric synchronization measured using MEG. Neuroimage *29*, 783–788. https://doi.org/10.1016/j.neuroimage.2005.08.048.
20. Leocani, L., Locatelli, T., Martinelli, V., Rovaris, M., Falautano, M., Filippi, M., Magnani, G., and Comi, G. (2000). Electroencephalographic coherence analysis in multiple sclerosis: correlation with clinical, neuropsychological, and MRI findings. J. Neurol. Neurosurg. Psychiatry *69*, 192–198. https://doi.org/10.1136/jnnp.69.2.192.
21. Van der Meer, M.L., Tewarie, P., Schoonheim, M.M., Douw, L., Barkhof, F., Polman, C.H., Stam, C.J., and Hillebrand, A. (2013). Cognition in MS correlates with resting-state oscillatory brain activity: An explorative MEG source-space study. Neuroimage. Clin. *2*, 727–734. https://doi.org/10.1016/j.nicl.2013.05.003.
22. Neuper, C., and Pfurtscheller, G. (2001). Event-related dynamics of cortical rhythms: frequency-specific features and functional correlates. Int. J. Psychophysiol. *43*, 41–58. https://doi.org/10.1016/S0167-8760(01)00178-7.
23. Pathak, A., Sharma, V., Roy, D., and Banerjee, A. (2022). Biophysical mechanism underlying compensatory preservation of neural synchrony over the adult lifespan. Commun. Biol. *5*, 567. https://doi.org/10.1038/s42003-022-03489-4.
24. Pathak, A., Roy, D., and Banerjee, A. (2022). Whole-Brain Network Models: From Physics to Bedside. Front. Comput. Neurosci. *16*, 866517. https://doi.org/10.3389/fncom.2022.866517.
25. Gonçalves, P.J., Lueckmann, J.-M., Deistler, M., Nonnenmacher, M., Öcal, K., Bassetto, G., Chintaluri, C., Podlaski, W.F., Haddad, S.A., Vogels, T.P., et al. (2020). Training deep neural density estimators to identify mechanistic models of neural dynamics. Elife *9*, e56261. https://doi.org/10.7554/eLife.56261.
26. Hashemi, M., Vattikonda, A.N., Sip, V., Guye, M., Bartolomei, F., Woodman, M.M., and Jirsa, V.K. (2020). The Bayesian Virtual Epileptic Patient: A probabilistic framework designed to infer the spatial map of epileptogenicity in a personalized large-scale brain model of epilepsy spread. Neuroimage *217*, 116839. https://doi.org/10.1016/j.neuroimage.2020.116839.
27. Hashemi, M., Vattikonda, A.N., Jha, J., Sip, V., Woodman, M.M., Bartolomei, F., and Jirsa, V.K. (2023). Amortized Bayesian inference on generative dynamical network models of epilepsy using deep neural density estimators. Neural Netw. *163*, 178–194. https://doi.org/10.1016/j.neunet.2023.03.040.
28. Cranmer, K., Brehmer, J., and Louppe, G. (2020). The frontier of simulation-based inference. Proc. Natl. Acad. Sci. USA *117*, 30055–30062. https://doi.org/10.1073/pnas.1912789117.
29. Sorrentino, P., Rucco, R., Lardone, A., Liparoti, M., Troisi Lopez, E., Cavaliere, C., Soricelli, A., Jirsa, V., Sorrentino, G., and Amico, E. (2021). Clinical connectome fingerprints of cognitive decline. Neuroimage *238*, 118253. https://doi.org/10.1016/j.neuroimage.2021.118253.
30. Genovese, A.V., Hagemeier, J., Bergsland, N., Jakimovski, D., Dwyer, M.G., Ramasamy, D.P., Lizarraga, A.A., Hojnacki, D., Kolb, C., Weinstock-Guttman, B., and Zivadinov, R. (2019). Atrophied Brain T2 Lesion Volume at MRI Is Associated with Disability Progression and Conversion to Secondary Progressive Multiple Sclerosis. Radiology *293*, 424–433. https://doi.org/10.1148/radiol.2019190306.
31. Shanahan, M. (2010). Metastable chimera states in community-structured oscillator networks. Chaos *20*, 013108. https://doi.org/10.1063/1.3305451.
32. D'Angelo, E., and Jirsa, V. (2022). The quest for multiscale brain modeling. Trends Neurosci. *45*, 777–790. https://doi.org/10.1016/j.tins.2022.06.007.
33. Selivanov, A.A., Lehnert, J., Dahms, T., Hövel, P., Fradkov, A.L., and Schöll, E. (2012). Adaptive synchronization in delay-coupled networks of Stuart-Landau oscillators. Phys. Rev. E Stat. Nonlin. Soft Matter Phys. *85*, 016201. https://doi.org/10.1103/PhysRevE.85.016201.
34. Hashemi, M., Vattikonda, A.N., Sip, V., Diaz-Pier, S., Peyser, A., Wang, H., Guye, M., Bartolomei, F., Woodman, M.M., and Jirsa, V.K. (2021). On the influence of prior information evaluated by fully Bayesian criteria in a personalized whole-brain model of epilepsy spread. PLoS Comput. Biol. *17*, e1009129. https://doi.org/10.1371/journal.pcbi.1009129.
35. Vattikonda, A.N., Hashemi, M., Sip, V., Woodman, M.M., Bartolomei, F., and Jirsa, V.K. (2021). Identifying spatio-temporal seizure propagation patterns in epilepsy using Bayesian inference. Commun. Biol. *4*, 1244. https://doi.org/10.1038/s42003-021-02751-5.
36. Deco, G., Ponce-Alvarez, A., Mantini, D., Romani, G.L., Hagmann, P., and Corbetta, M. (2013). Resting-State Functional Connectivity Emerges from Structurally and Dynamically Shaped Slow Linear Fluctuations. J. Neurosci. *33*, 11239–11252. https://doi.org/10.1523/JNEUROSCI.1091-13.2013.
37. Sunnåker, M., Busetto, A.G., Numminen, E., Corander, J., Foll, M., and Dessimoz, C. (2013). Approximate Bayesian Computation. PLoS Comput. Biol. *9*, e1002803. https://doi.org/10.1371/journal.pcbi.1002803.
38. Thompson, A.J., Banwell, B.L., Barkhof, F., Carroll, W.M., Coetzee, T., Comi, G., Correale, J., Fazekas, F., Filippi, M., Freedman, M.S., et al. (2018). Diagnosis of multiple sclerosis: 2017 revisions of the McDonald criteria. Lancet Neurol. *17*, 162–173. https://doi.org/10.1016/S1474-4422(17)30470-2.
39. Smith, S.M., Jenkinson, M., Woolrich, M.W., Beckmann, C.F., Behrens, T.E.J., Johansen-Berg, H., Bannister, P.R., De Luca, M., Drobnjak, I., Flitney, D.E., et al. (2004). Advances in functional and structural MR image analysis and implementation as FSL. Neuroimage *23*, S208–S219. https://doi.org/10.1016/j.neuroimage.2004.07.051.
40. Leemans, A., and Jones, D.K. (2009). The B-matrix must be rotated when correcting for subject motion in DTI data. Magn. Reson. Med. *61*, 1336–1349. https://doi.org/10.1002/mrm.21890.
41. Smith, S.M. (2002). Fast robust automated brain extraction. Hum. Brain Mapp. *17*, 143–155. https://doi.org/10.1002/hbm.10062.
42. Klein, A., and Tourville, J. (2012). 101 Labeled Brain Images and a Consistent Human Cortical Labeling Protocol. Front. Neurosci. *6*, 171. https://doi.org/10.3389/fnins.2012.00171.
43. Friston, K.J., Ashburner, J., Frith, C.D., Poline, J.-B., Heather, J.D., and Frackowiak, R.S.J. (1995). Spatial registration and normalization of images. Hum. Brain Mapp. *3*, 165–189. https://doi.org/10.1002/hbm.460030303.
44. Schmidt, P., Gaser, C., Arsic, M., Buck, D., Förschler, A., Berthele, A., Hoshi, M., Ilg, R., Schmid, V.J., Zimmer, C., et al. (2012). An automated tool for detection of FLAIR-hyperintense white-matter lesions in Multiple Sclerosis. Neuroimage *59*, 3774–3783. https://doi.org/10.1016/j.neuroimage.2011.11.032.
45. Ashburner, J. (2007). A fast diffeomorphic image registration algorithm. Neuroimage *38*, 95–113. https://doi.org/10.1016/j.neuroimage.2007.07.007.
46. Sorrentino, P., Rucco, R., Baselice, F., De Micco, R., Tessitore, A., Hillebrand, A., Mandolesi, L., Breakspear, M., Gollo, L.L., and Sorrentino, G. (2021). Flexible brain dynamics underpins complex behaviours as observed in Parkinson's disease. Sci. Rep. *11*, 4051.
47. Oostenveld, R., Fries, P., Maris, E., and Schoffelen, J.-M. (2011). FieldTrip: open source software for advanced analysis of MEG, EEG, and invasive electrophysiological data. Intell. Neurosci. *2011*, 156869. https://doi.org/10.1155/2011/156869.
48. Gross, J., Baillet, S., Barnes, G.R., Henson, R.N., Hillebrand, A., Jensen, O., Jerbi, K., Litvak, V., Maess, B., Oostenveld, R., et al. (2013). Good practice for conducting and reporting MEG research. Neuroimage *65*, 349–363. https://doi.org/10.1016/j.neuroimage.2012.10.001.
49. Sadasivan, P.K., and Dutt, D. (1996). SVD based technique for noise reduction in electroencephalographic signals. Signal Process. *55*, 179–189. https://doi.org/10.1016/S0165-1684(96)00129-6.
50. de Cheveigné, A., and Simon, J.Z. (2008). Denoising based on spatial filtering. J. Neurosci. Methods *171*, 331–339. https://doi.org/10.1016/j.jneumeth.2008.03.015.
51. Barbati, G., Porcaro, C., Zappasodi, F., Rossini, P.M., and Tecchio, F. (2004). Optimization of an independent component analysis approach for artifact identification and removal in magnetoencephalographic signals. Clin. Neurophysiol. *115*, 1220–1232. https://doi.org/10.1016/j.clinph.2003.12.015.
52. Nolte, G. (2003). The magnetic lead field theorem in the quasi-static approximation and its use for magnetoencephalography forward calculation in realistic volume conductors. Phys. Med. Biol. *48*, 3637–3652.
53. Hillebrand, A., Tewarie, P., van Dellen, E., Yu, M., Carbo, E.W.S., Douw, L., Gouw, A.A., van Straaten, E.C.W., and Stam, C.J. (2016). Direction of information flow in large-scale resting-state networks is frequency-dependent. Proc. Natl. Acad. Sci. USA *113*, 3867–3872. https://doi.org/10.1073/pnas.1515657113.
54. Hayes, M.H. (1996). Statistical Digital Signal Processing and Modeling (John Wiley & Sons), pp. 391–493.

55. Reissig, R. (1967). A. A. Andronov, A. A. Vitt, and S. E. Khaikin, Theory of Oscillators. (International Series of Monographs in Physics, Vol. 4) XXXII + 815 S. m. 598 Fig. Oxford/London/Edinburgh/New York/Toronto/Paris/Frankfurt 1966. Pergamon Press. Preis geb. £ 10 net. Z. Angew. Math. Mech. *47*, 480–481. https://doi.org/10.1002/zamm.19670470720.

56. Liu, Q., Xu, J., Jiang, R., and Wong, W.H. (2021). Density estimation using deep generative neural networks. Proc. Natl. Acad. Sci. USA *118*, e2101344118. https://doi.org/10.1073/pnas.2101344118.

57. Papamakarios, G., Pavlakou, T., and Murray, I. (2017). Masked autoregressive flow for density estimation. In Proceedings of the 31st International Conference on Neural Information Processing Systems NIPS'17, R. Garnett, ed. (Curran Associates Inc), pp. 2335–2344.

58. Tejero-Cantero, A., Boelts, J., Deistler, M., Lueckmann, J.-M., Durkan, C., Gonçalves, P., Greenberg, D., and Macke, J. (2020). sbi: A toolkit for simulation-based inference. J. Open Source Softw. *5*, 2505. https://doi.org/10.21105/joss.02505.

59. Hashemi, M., Hutt, A., Buhry, L., and Sleigh, J. (2018). Optimal Model Parameter Estimation from EEG Power Spectrum Features Observed during General Anesthesia. Neuroinform *16*, 231–251. https://doi.org/10.1007/s12021-018-9369-x.

60. Belsley, D.A., Kuh, E., and Welsch, R.E. (2005). Regression Diagnostics: Identifying Influential Data and Sources of Collinearity (John Wiley & Sons), pp. 85–191.

61. Snee, R.D. (1983). Regression Diagnostics: Identifying Influential Data and Sources of Collinearity. J. Qual. Technol. *15*, 149–153. https://doi.org/10.1080/00224065.1983.11978865.

STAR★METHODS

KEY RESOURCES TABLE

REAGENT or RESOURCE	SOURCE	IDENTIFIER
Software and algorithms		
Code used for the analysis	https://github.com/ins-amu/virtual_ms	N/A
Fieldtrip	https://github.com/fieldtrip/fieldtrip	Article: https://doi.org/10.1155/2011/156869
LST	https://github.com/CompImg/LST-AI	Article: https://www.ncbi.nlm.nih.gov/pmc/articles/PMC6865732/
CAT	https://github.com/ChristianGaser/cat12	Article: https://www.sciencedirect.com/science/article/abs/pii/S0730725X09000149
Scikit-learn	https://github.com/scikit-learn/scikit-learn	Article: https://jmlr.csail.mit.edu/papers/v12/pedregosa11a.html
SBI	https://github.com/sbi-dev/sbi	Article: https://joss.theoj.org/papers/10.21105/joss.02505
TVB	https://www.thevirtualbrain.org/tvb/zwei	Article: https://www.frontiersin.org/articles/10.3389/fninf.2013.00010/full

RESOURCE AVAILABILITY

Lead contact

Pierpaolo Sorrentino (pierpaolo.sorrentino@univ-amu.fr).

Materials availability

Given the personal nature of the data, it is not possible to make it public. However, the data is available upon request to the corresponding authors for the purpose of replication.

Data and code availability

- Given the clinical nature of the data, it is not possible to make the data public. However, the data is available upon request to the corresponding authors for the purpose of replication.
- The code is publicly available at https://github.com/ins-amu/virtual_ms
- Any additional information required to reanalyze the data reported in this work paper is available from the lead contact upon request.

EXPERIMENTAL MODEL AND STUDY PARTICIPANT DETAILS

The participants were recruited at the outpatient clinic of the Institute for Diagnosis and Cure Hermitage Capodimonte (Naples, Italy). MS was diagnosed according to the revised 2017 McDonald criteria,[38] with exclusion criteria defined as age <18 years, recent clinical relapse and/or steroid therapy (i.e., 3 months before the study), use of illicit drugs, stimulants, amphetamines, barbiturates, and cannabinoids; history of central nervous system disorders other than MS, severe mental illness, inability to understand and complete "patient reported outcomes" and cognitive evaluation, or inability to undergo the MRI scan. All patients underwent a neurological clinical examination, Expanded Disability Status Scale (EDSS) scoring, the Symbol Digit Modalities Test (SDMT) to measure cognitive impairment, the Fatigue Severity Scale (FSS), and the Beck Depression Inventory (BDI) to assess depression. The controls for the MS cohort were selected among the caregivers and spouses of the patients. Genetic relatives were not allowed as controls. The main features of the MS cohort are summarized in Table 1, while detailed information is reported in Table S1. The research was conducted in accordance with the Declaration of Helsinki. A written informed consent was obtained from subjects after explanation of the study was approved by the local Ethics Committee (Prot.n.93C.E./Reg. n.14-17OSS).

METHOD DETAILS

MRI acquisition and processing

The data was processed as in Sorrentino et al.[13] In short, each MRI scan was performed immediately after the MEG recording (Figure 1A) on the same MRI scanner (1.5 Tesla, Signa, GE Healthcare). Analyzed MRI sequences included a 3D-FLAIR volume (TR/TE/TI 7000/145/1919 ms, echo train length 170, Acquisition matrix 512 × 512 × 212, sagittal partitions, voxel size 0.52 × 0.52 × 0.80 mm^3) and a T1-weighted 3D-volume

(Fast Spoiled Gradient-Echo, TR/TE/TI 7.1/2.0/450 ms, Flip Angle 10°, Acquisition matrix 256 × 256 × 162, sagittal partitions, voxel size 1 × 1 × 1 mm^3). Each FLAIR volume was rigid-body coregistered. Echo-planar imaging was used for DTI reconstruction (TR/TE 12,000/95.5 ms, voxel 0.94 × 0.94 × 2.5 mm^3, 32 equally spaced diffusion-sensitizing directions, 5 B0 volumes) and 3D-FLAIR volume for WM lesion segmentation (TR/TE/TI 7000/145/1919 ms, echo train length 170, 212 sagittal partitions, voxel size 0.52 × 0.52 × 0.80 mm^3). Preprocessing of the diffusion MRI data was carried out using the software modules provided in the FMRIB software library (FSL, http://fsl.fmrib.ox.ac.uk/fsl). All diffusion MRI datasets were corrected for head movements and eddy current distortions using the "eddy_correct" routine,[39] rotating the diffusion sensitizing gradient directions accordingly,[40] and a brain mask was obtained from the B0 images using the Brain Extraction Tool routine.[41] A diffusion-tensor model was fitted at each voxel, and fiber tracts were generated over the whole brain by deterministic tractography using the Fiber Assignment by Continuous Tracking (FACT) algorithm implemented in Diffusion Toolkit (angle threshold 45°, spline-filtered, masking by the FA maps thresholded at 0.2). A cortical study-specific Region of Interest (ROI) datasets was obtained by masking the ROIs available in an MNI space-defined volumetric version of the Desikan-Killiany-Tourville (DKT) ROI atlas[42] using the GM tissue probability map available in SPM (thresholded at 0.2). This was done to limit the endpoints of the fibers to cortical and adjacent juxtacortical white matter voxels in the subsequent ROI-based analysis of the tractography data. To obtain the corresponding patient-specific ROI sets, each participant's FA volume was spatially normalized[43] to the FA template provided by FSL using SPM12, and the resulting normalization matrices were inverted and applied to the ROI set. MS lesions were segmented using the lesion prediction algorithm[44] implemented in the Lesion Segmentation Tool (LST toolbox version 3.0.0; www.statistical-modeling.de/lst.html). Based on the resulting lesion maps, a lesion-filling procedure based on the intensity distribution of the normal-appearing white matter surrounding each lesion was applied to each T1-weighted volume using an LST routine, to avoid lesion-related segmentation bias, and the resulting lesion-filled T1-weighted 3D volume was segmented in GM, WM, and CSF and normalized to the MNI space using a fast diffeomorphic registration algorithm (Diffeomorphic Anatomical Registration using Exponentiated Lie algebra, DARTEL[45]), as implemented in the Computational Anatomy Toolbox (CAT12, https://neuro-jena.github.io/cat/). The global atrophy was defined as the sum of the gray and white matter volume divided by the intracranial volume.

MEG pre-processing

MEG pre-processing and source reconstruction were performed as in Ashburner.[46] Preprocessing and source reconstruction operations were carried using the Fieldtrip Toolbox.[47] Each participant underwent a MEG recording, composed of both eyes-closed resting-state segments of 3'30" each. Four anatomical coils were applied on the head of each participant and their position was recorded along with the position of four head anatomical points, to identify the position of the head during the recording. Eye blinking (if present) and heart activity were recorded through electro-oculogram (EOG) and electrocardiogram (ECG), to identify physiological artifacts.[48] An expert rater checked for noisy signals and removed them. In particular, channels with high-frequency or high-amplitude noise, with remainders of physiological artifacts, with movement artifacts were removed. Time interval with high environmental noise were also removed. An anti-alias filter was applied to the MEG signals, acquired at 1024 Hz, before being filtered with a fourth order Butterworth IIR band-pass filter (0.5–48 Hz). We used principal component analysis[49,50] and supervised independent component analysis[51] to remove the environmental noise and the physiological artifacts, respectively.

Source reconstruction

The source reconstruction was performed as in Sorrentino et al.[13] In brief, the signal time series were reconstructed using 84 ROIs based on the DKT atlas. The reconstruction took place utilizing the volume conduction model proposed by Nolte.[52] Based on the native MRIs of each subject, the linearly constrained minimum variance (LCMV) beamformer was applied to reconstruct the signal sources based on the centroids of each ROI.[53]

Power-spectra estimation

Power spectral density (PSD) for each source-reconstructed time-series was estimated by the Welch method as implemented in MATLAB.[54] In short, each time-series is divided into the longest possible segments to obtain as close to but not exceed 8 segments with 50% overlap.[54] Each segment is windowed with a Hamming window. The modified periodograms are then averaged to obtain the PSD estimate.[54] The resulting PSD estimates were further grouped across ROIs to obtain a median PSD for each participant. The peak alpha frequency, peak alpha spectral density and total alpha power (area under the spectral density curve between 8 and 13 Hz) were estimated from the resulting median PSD. Differences between groups were tested using the Mann-Whitney U-test, and then Bonferroni corrected across the three parameters explored.

Numerical solution of the stuart - Landau model

Each ROI was conceptualized as an autonomous Stuart-Landau oscillator, Figure 1B.[17,33,55] The Stuart-Landau system possesses either damped or limit-cycle solutions, depending on the bifurcation parameter a.[55] For $a<0$, the system exhibits damped oscillations, akin to a pendulum subject to friction. In response to noise, the system relaxes back to its stable fixed point by executing oscillations specified by angular frequency ω_0 . The rate of amplitude damping is dictated by $|a|$. In contrast, limit cycle solutions exist for $a>0$; in this regime, the system can oscillate in a self-sustained fashion, even in the absence of external noise. Oscillators are connected to each other via white-matter, with coupling strength specified by the (subject-specific) DTI fiber counts (c_{jk}). Adjacency matrices are scaled by a global coupling parameter

(G). Coupling between ROIs is subject to finite conduction times, estimated by dividing inter-node Euclidean distances by an average conduction velocity, $\tau_{jk} = \frac{d_{jk}}{v_{jk}}$. For simplicity, we assume a common cortico-cortical conduction velocity to estimate distance dependent averaged velocities ($v_{jk} = v$). The activity of each ROI is given as:

$$\dot{Z}_j = Z_j\left(a + i\omega_j - |Z_j|^2\right) + G\sum_{j\neq k}^{N} c_{jk}\left[Z_k\left(t - \tau_{jk}\right) - Z_j(t)\right] + \beta\left(\eta_1^j + i\eta_2^j\right) \quad \text{(Equation 1)}$$

Where Z is a complex variable, and $Re[Z(t)]$ is the corresponding time-series. Each ROI has a natural frequency of 40 Hz ($\omega_j = \omega_0 = 2 * \pi * 40$). This choice of natural frequency is motivated by empirical studies that demonstrate how gamma oscillations emerge from a balance of excitation and inhibition and play a role in local circuit computations. This study is conducted with $a = -5$, to capture the highly variable amplitude envelope of gamma oscillations observed in experimental recordings. Moreover, $a = -5$ best captures the slowest decay time constants of $GABA_B$ inhibitory receptors (~1s).[16] Noise, with noise factor $\beta = 1$ was added to each oscillator to model stochastic fluctuations.

The expected spectral summary statistics were calculated (Figures 1C and 1D), applying machine learning techniques to large-scale models of the brain, given *a priori* range of parameters. The deep neural network was built to be invertible, meaning that, once trained, it can generate spectral properties from the velocities, as well as estimating the velocities from the spectral properties. Then, the empirical spectral properties were used as the input to the 'reversed' algorithms (conveyed by the reversed gradient of colors in Figure 1), which provided us with the most likely conduction velocity (in each subject). The inferred velocities were then added to a multilinear model, along with demographic, clinical and structural information, in order to predict the individual disability.

Since the object of the study is to model alpha oscillations, we restrict our attention to the regime spanned by $G = 800 - 2000$ and $V = 1 - 20\frac{m}{s}$ (see Figures 3, 4, and 5). Simulations were run for 100s by numerically integrating the system of equations (Equation 1), through the Euler-Murayama method. The first 10s were discarded as transients. The PSD was estimated for the remaining 90s, using the *pwelch* function. This process was repeated for each subject's connectome to infer the subject-specific optimal working point.

QUANTIFICATION AND STATISTICAL ANALYSIS

Simulation-based inference on whole-brain parameters

Next, we use probabilistic machine learning based on a large-scale brain network model of MEG to infer the individual conduction velocities in MS patients (and controls). In brief, we built a function that, given any particular averaged velocity (and coupling parameter), provides us with the expected peak-frequency, peak-amplitude and total power in the alpha band. The key point is that such a function is required to be smooth and invertible. Hence, we then invert this function to estimate the most likely individual velocities (and coupling parameter), given the observed individual spectral-features.

More in detail, the Bayesian approach we use offers a principled method to perform probabilistic inference and prediction (Figures 1F–1I), while the uncertainty in the parameter estimation is naturally quantified through probability distributions placed on the parameters updated with the information provided by the data. Formally, given data y and model parameters θ, Bayes rule defines the posterior distribution as $p(\theta|y) \propto p(y|\theta)\ p(\theta)$, where $p(\theta)$ is the prior probability distribution (over a plausible range of values), and $p(y|\theta)$ is the likelihood distribution, which quantifies the probability that the observation y is generated by a specific set of θ. Here, $\theta = \{G, V\}$, with G defined as the global coupling and V as the average conduction velocities across the white matter bundles, whereas y represents the PSD features (peak frequency, peak amplitude and total power in the alpha band), observed in the MEG data of each subject.

The key challenge to efficiently perform Bayesian inference lies in the evaluation of the likelihood function $p(y|\theta)$, given the samples from the prior distribution. In other words, one needs the calculation of intractable integrals to evaluate the likelihood of observing y given a certain value of θ (that is, the delays and coupling). In particular, for inference on MEG data at the whole-brain scale, the computational cost of evaluating the likelihood function becomes prohibitive, rendering the likelihood-based approaches, such as Markov chain Monte Carlo sampling, inefficient in practice.[27] Simulation-based inference (SBI), or likelihood-free inference, performs efficient Bayesian inference for high-dimensional complex models where the calculation of the likelihood function is either analytically or computationally intractable.[28] SBI employs deep artificial neural networks (ANNs) to learn an invertible transformation between parameters and data features from a budget of simulations performed with parameters randomly drawn from the prior distribution (as opposed to sampling from the prior distribution and then explicitly evaluating the likelihood function). Using this approach, a simple baseline probability distribution (e.g., a uniform or standard normal distribution) is converted into a more complex distribution (i.e., posterior distribution), through a sequence of invertible transformations (implemented via deep neural networks). In this context, density estimators reconstruct the probability density function (i.e., the relationship between the outcomes of a random variable and its probability) using a set of given data points, without having access to all the possible outcomes. Traditional density estimators such as histograms and kernel density estimators typically perform well only for a small number of random variables. In contrast, recently advanced neural density estimators based on ANNs scale better with the number of random variables, and can incorporate domain knowledge in their design.[56] In this study, we used a Masked Autoregressive Flow (MAF),[57] which supports invertible nonlinear transformations, and enables highly expressive transformations with low-cost computation. In the implementation, the MAF model consists of 5 autoregressive layers, each with two hidden layers, and each hidden layer contains 50 units.

In our case, to perform SBI, three inputs need to be specified: (i) a prior distribution describing the possible conduction velocities (and global coupling), (ii) a mechanistic model that simulates the large-scale activity in case of any particular conduction velocity and global

coupling (here, the Stuart-Landau model coupled according to the individual connectomes) and, (iii) a set of observed MEG data (or low-dimensional data features) as the target of the fitting (in this context, the observed spectral features). We trained a MAF with a budget of simulations given random parameters drawn from the priors. After the training step, one can quickly evaluate the posterior distribution for arbitrary new observations or empirical data by a forward pass through the trained MAF. By providing fast model simulations and extracting informative but low-dimensional data features (such as the PSD), this methodology efficiently provides the posterior distribution of model parameters at the whole-brain scale,[27] since it requires neither model nor data features to be differentiable.[25] For training the MAF, assuming that our dataset has samples $\{(\theta_i, y_i)\}_{i=1}^{N}$, with parameters drawn from the prior, and the observations generated from the forward model, the posterior is obtained by minimizing the loss function

$$Loss(\psi) = -\sum_{i=1}^{N} log\, q_{F(y_i,\psi)}(\theta_i)$$

over network parameters ψ. After the parameters of the neural networks are optimized, for new observation y_{obs}, we can efficiently estimate the target posterior $p(\theta|y_{obs})$ by $q_{F(y=y_{obs},\psi)}(\theta)$, which refers to the (approximated) variational distribution.

After the training step and the posterior estimation, we proceeded to the sensitivity analysis by calculating the eigenvalues and the corresponding eigenvectors[25] from:

$E_{p(\theta|y_{obs})}[\nabla_\theta\, p(\theta|y_{obs})^T \nabla_\theta\, p(\theta|y_{obs})]$, and then an eigendecomposition: $M = Q\Lambda|Q^{-1}$.

This approach, known as the active subspace, focuses on the expected value (denoted by E) of the outer product of the posterior gradient with itself at y_{obs}, averaged over all possible values of θ, according to the posterior distribution $p(\theta|y_{obs})$. In other words, it quantifies how the posterior density varies with changes in the parameters, considering the uncertainty in the observed data. A strong eigenvalue indicates that the gradient of the posterior is large and, hence, the system output is sensitive to changes along the direction of the corresponding eigenvector. This will allow us to compare the relative importance of the two inferred parameters (i.e., the velocities and the global coupling) on the outcome measures (i.e., the observed spectral properties).

In this study, the SBI on the whole-brain model of Stuart-Landau oscillators is first validated using synthetic data generated with the subject-specific structural connectomes, as to recover the ground-truth parameters, and then applied to empirical MEG data. To this end, we used the PyTorch-based SBI package,[58] and a simulation budget size of 5000 simulations (unless otherwise specified), in order to train the MAF. The parameters were drawn randomly from a uniform prior in the ranges: $G \in [800, 2000]$, and $V \in [1, 20]$. For model simulation, we used Euler integration with a time step of dt = $1e^{-4}$ sec. The model output has been smoothed using a Savitzky-Golay filter (window size = 5 msec, order = 3) to enhance the accuracy of data feature calculations. By transforming the observation from the time-domain to the frequency-domain,[59] we utilized the summary statistics of PSD (amplitude, median frequency, and the total alpha power) as the data feature for the training and the inference steps. This was done, as explained earlier, based on the relationship we demonstrated to exist between the velocities in Stuart-Landau oscillators (weakly coupled according to the patient's connectome), and the frequency of oscillations across the network. The model simulation and parameter estimation were performed on a Linux machine with Intel Core i9-10900 CPU 2.80 GHz and 64 GB of RAM.

Prediction of clinical impairment via a multimodal linear model

We then moved on to test the hypothesis that the inferred velocities could improve the prediction of the individual clinical impairment as compared to only including the total volume load in the whole-brain model (Figures 1J, 1K, and 1L). To test this hypothesis, we built a multilinear model to predict the individual clinical disability (as estimated by the EDSS) based on the demographics, the clinical data and the total lesion load. Specifically, we considered the EDSS, after a rank-based inverse normal transformation (in order to resample the data to a normal distribution), as a dependent variable, while age, gender, disease duration and lesion load (i.e., the total volume of the lesions) were considered as predictors. A logarithmic transformation was applied to the lesion load. Multicollinearity was assessed through the variance inflation factor (VIF).[60,61] Given the relatively low numerosity of our sample, we validated our model using the leave-one-out cross-validation (LOOCV). Hence, we built *n* multilinear model (where *n* is the size of the sample), each time excluding a different subject from the training set, and then verifying the ability of the model to predict the clinical disability of the excluded subject. We have repeated the same scheme, substituting the brain atrophy to the lesion load as a predictor.